Journal of Solid State Chemistry **156,** 394–399 (2001)
doi:10.1006/jssc.2000.9011, available online at http://www.idealibrary.com on IDEAL®

# Computer Simulations of Thermal Expansion in Lanthanum-Based Perovskites

R. E. Williford, J. W. Stevenson, S.-Y. Chou, and L. R. Pederson

*Pacific Northwest National Laboratory, P.O. Box 999, Richland, Washington, 99352*

Received December 27, 1999; in revised form October 18, 2000; accepted October 27, 2000

**Differential thermal expansion is important when two strongly bonded ceramics are subjected to high temperatures, as in solid oxide fuel cells. Free energy minimization (EM) and molecular dynamics (MD) techniques were used to simulate the thermal expansion of the perovskites $(La, Ca)CrO_3$ and $(La, Sr)(Co, Fe)O_3$ on the atomistic scale. This paper explores the use of empirical partial charge interatomic potentials to represent the partially covalent bonding in these materials. The EM simulations underpredicted the thermal expansion coefficients (CTEs) by up to 26% due to limitations in the potentials. The MD simulations predicted the CTEs to within 17% of experimental data for $(La, Ca)CrO_3$. MD predictions of the CTEs for $(La, Sr)(Co, Fe)O_3$ were significantly lower than the experimental data due to the approximate nature of the $Co^{4+}$ and $Fe^{4+}$ interatomic potentials. Improvements in these results are possible if more extensive databases become available for refining the potentials and effective charges.** 

*Key Words:* **lanthanum calcium chromite; lanthanum strontium cobalt iron oxide; free energy minimization; molecular dynamics; thermal expansion; partial charge models.**

## 1. INTRODUCTION

Solid oxide fuel cells (SOFCs) are composed of several basic elements (electrodes, electrolytes, and interconnects). These are often configured in a stack composed of alternating layers of materials. The materials must not only exhibit high electronic conductivity but must also withstand some rather severe operating conditions: extremely oxidizing or reducing atmospheres at temperatures on the order of 1000°C. Consequently, the materials of choice are often ceramics.

The ceramic materials in a SOFC stack are intimately bonded together to ensure good electrical contacts. However, the high temperatures cause appreciable thermal expansions. The different component materials naturally lead to differential thermal expansions and thus to thermal stresses that can cause fracture. The fractures then provide unrestricted gas paths between the fuel and air, consequently destroying the primary function of the fuel cell. It is thus important to select materials with matched thermal expansion coefficients (CTEs).

The experimental approach to optimize the CTEs can be expensive because many materials must be tested. In addition, depending on the experimental technique, it can be difficult to separate the CTE from other expansion phenomena, such as defect-induced chemical expansions caused by reducing atmospheres. One method of reducing these costs is to develop computational tools that can be used to predict the CTEs for a given stoichiometry and then use fewer experiments to verify those predictions. This paper is an initial attempt at the development of such predictive computational tools.

The CTE depends on the bulk modulus ($B$). From a continuum viewpoint, the relationship is

$$\mathrm{CTE} = GC_v/VB, \qquad [1]$$

where $G$ is the Gruneisen constant (nearly independent of temperature), $C_v$ is the specific heat at constant volume, and $V$ is volume. From an atomistic viewpoint, this dependence is manifested in the relationship between the elastic properties and the curvatures of the interatomic potentials and how these potentials determine thermal expansion behavior. An objective of this paper is to develop interatomic potentials that are capable of reproducing the measured bulk moduli of these materials and thus attempt to improve the prediction of the thermal expansion coefficients.

The ceramics of choice for SOFC applications are often $ABO_3$ perovskites because their electrical properties (and sometimes their structures) can be manipulated to advantage through the use of dopants. The perovskites are interesting because, despite intense interest over the past decade, there remain some outstanding questions concerning the chemical character of the $A$ site and the amount of covalency associated with the $B$ site (1). In recent work (2, 3),



0022-4596/01 $35.00

indications were found that partial charge models may be useful for simulating the thermal expansion coefficients of calcium- and strontium-doped lanthanum chromites. Similar results have also been found by others (1) for strontium titanate. A partial charge is less than the formal charge (e.g., $-1.6\ |e|$ for oxygen rather than the formal $-2.0\ |e|$) and approximates the effects of partially covalent bonding. In the present paper, we develop partial charge models for two perovskites of importance for fuel cells: $(La,Ca)CrO_3$ and $(La,Sr)(Co,Fe)O_3$. The perovskite $(La,Ca)CrO_3$ has been considered as a SOFC interconnect material because of its relatively high electronic conductivity and its stability in both oxidizing and reducing atmospheres. The perovskite $(La,Sr)(Co,Fe)O_{3-\delta}$ exhibits substantial mixed electronic–ionic conduction at high temperatures (4) and has been considered as a candidate for fuel cell cathodes, oxygen separation membranes, and membrane reactors for syngas production.

## 2. EXPERIMENTAL MATERIALS AND DATA

For brevity of notation in the balance of the paper, the chromite material is described by the percentage acceptor substituted on the $A$ sites; i.e., 20% Ca in $(La,Ca)CrO_3$ is denoted LCC20. Descriptions of the sample preparation are given in Refs. (5) and (6) and summarized in previous papers (2, 3). Calculations were limited to the fully oxidized material (heated in air, denoted "ox") and the fully reduced material ($P(O_2) = 10^{-18}$ atm, denoted "red"). Complete oxidation was assumed for the oxidized cases (3). Lattice parameters for the oxidized and reduced cases and stoichiometric coefficients for the reduced cases (e.g., $La_{1-x}Ca_xCr^{3+}_{1-x+2\delta}Cr^{4+}_{x-2\delta}O_{3-\delta}[V_0]_\delta$) were developed in Refs. (2) and (3) using data from (5). The measured Young's modulus for the LCC20 material was obtained from (7), and the bulk modulus was estimated assuming isotropy and a Poisson's ratio of 0.28. The experimentally measured CTE value was obtained from (6), but data for LCC were available only for the oxidized case.

The $La_{1-x}Sr_xCo_{1-y}Fe_yO_{3-\delta}$ compositions are similarly described by the abbreviation LSCF, followed by four numerals referring to the proportion of each cation. For example, $La_{0.6}Sr_{0.4}Co_{0.2}Fe_{0.8}O_{3-\delta}$ is designated LSCF6428. Various compositions of the system $La_{1-x}Sr_xCo_{1-y}Fe_yO_{3-\delta}$ were prepared using the glycine–nitrate combustion synthesis technique (4). Phase development was determined using X-ray diffraction. Room temperature oxygen stoichiometries of calcined powder specimens were determined by iodometric titration using a modified version of Nadalin and Brozda's oxidizing power method No. 3 (8). The results were $\delta = 0.0$, 0.03, and 0.04 for LSCF6428, LSCF4628, and LSCF2828, respectively. A complete description of the sample preparation and characterization is given in Ref. (4). The bulk moduli of these specimens were measured by standard pulse-echo techniques using a Stavely Model 137 sonic tester. The experimental thermal expansion coefficient for LSCF6428 was obtained from (9).

## 3. COMPUTATIONAL METHODS

Two computational techniques were employed in this paper: static lattice free energy minimization (EM) and molecular dynamics (MD). Both methods used the Ewald sum technique for long-range Coulombic forces and Buckingham potentials for the short-range forces. Electrical neutrality was maintained exactly in the EM method and within $0.4\ |e|$ for a 1280-atom model in the MD method. The EM calculations were performed for an infinite crystal using mean field techniques, while the MD calculations used $4 \times 4 \times 4$ supercell realizations with random allocation of dopants and charge balancing species such as oxygen vacancies. A single realization was used for each of the MD cases; so the results must be considered as approximate. Periodic boundary conditions that reproduced the crystal symmetries were maintained for each case, and thermal expansions were calculated on a volumetric basis.

The EM technique employs the Born model and has been successfully used for the study of other perovskites (10–13). The General Utility Lattice Program (GULP) (14, 15) was used in this investigation, along with a shell model description of polarization (16). A simple harmonic spring model was used to represent the separation of the shell, which nominally represents the mean position of the valence electron cloud, from the ionic core (nucleus plus core electrons). Within an ion, the shell charge and spring constant combine to determine the overall electronic polarizability. The net ionic (core plus shell) charge may depart from formal charges to approximate the effects of partial covalency. GULP also contains a least-squares optimization technique for fitting potential parameters to structural data and physical properties, including the more reliable "relaxed fitting" method (15). This fitting capability was used to develop the potentials described below.

Total energy minimizations were performed with GULP for the zero Kelvin case, which was assumed to correspond to the experimental data at 298 K, within the uncertainty of the experimental data. Free energy minimizations were performed at higher temperatures using the quasiharmonic approximation with analytical free energy derivatives (17). The ZSISA method (zero static internal stress approximation) was used in this work, where only the strains are minimized with respect to the free energy and the internal degrees of freedom are minimized with respect to the internal energy (18). This approach has been found to be more stable at higher temperatures than total free energy

minimization. Furthermore, the zero point energy was excluded from the free energy to equivalence the free energy and internal energy calculations at absolute zero, since the potential parameters were derived statically. Phonon sampling was performed using a Monkhorst–Pack (19) shrinking factor of 4 along each crystal axis.

Energy minimization is a tool capable of computing the energetics of isolated defects in extended solids using the Mott–Littleton approximation (20) or for higher defect concentrations via the supercell approach. However, in the present paper the lattice expansions were atomistically simulated using an infinite-crystal mean field approximation, which is better suited for high concentrations of defects (i.e., substitutions) and their effects on macroscopic properties, since it avoids the difficulties associated with ensuring that all possible defect configurations are explicitly sampled. This means that the total interatomic potential at a particular site was the sum of potentials for all species (e.g., vacancies and/or substitutions) at that site, each weighted by their partial occupancies. The near-field potential cutoff radii were 10 Å for cation–oxygen interactions and 12 Å for oxygen–oxygen interactions, the latter being larger to allow for the longer ranged dispersion term.

Molecular dynamics (MD) calculations were also performed for comparison to the thermal expansion values computed from the output of the EM code. Although previous work (21) has shown that the two methods produce comparable results for simple materials like MgO, it is useful to check this result for perovskites, which have more degrees of freedom. The code used for this purpose was DL_POLY (22). This code is a well-documented package of routines for the simulation of a wide variety of MD problems and includes several NPT ensembles that were needed for simulating thermal expansion. The simulation model was a $4 \times 4 \times 4$ unit cell with periodic boundary conditions that mimic the crystal symmetry in each case (1280 atoms for orthorhombic LCC20, 320 atoms for cubic LSCF6428). This supercell size was chosen because it corresponds to the equivalent phonon sampling obtained by a shrinking factor of 4 in the free energy minimization approach. The doped LCC systems were modeled by substituting 20% Ca at random La sites in the lattice and $Cr^{4+}$ at random $Cr^{3+}$ sites (for charge compensation in this material) and randomly removing the stoichiometrically prescribed number of oxygens to provide charge compensating vacancies for the reduced cases. A similar approach was used for LSCF6428. The shell model potentials used were the same as those used in the EM calculations. The cutoff radii for the potentials were 10 Å for LCC20 and 7 Å for LSCF6428. The smaller cutoff for the LSCF was required because of the smaller supercell dimensions, and the results must therefore be considered as approximate. The EM and MD techniques are both sensitive to the details of the interatomic potentials, which are discussed next.

## 4. INTERATOMIC POTENTIALS

Previous results (2) indicated that partial charge models seemed suitable for approximate representations of the partially covalent bonding present in lanthanum chromites. Such partial charge models can more accurately reproduce the bulk moduli of perovskites and may thus improve predictions of the thermal expansion. Similar results have been found for strontium titanate (1). Based on those results, the LCC potentials were developed by starting with a set of potentials previously used for chromites (3) and refitting to the LCC20 structure and bulk modulus. The resulting potentials and core–shell charges are shown in Tables 1 and 2 and in Fig. 1. The LSCF potentials were similarly refit starting with potentials developed for other perovskites (10, 23) and are shown in Tables 3 and 4 in Fig. 2. All potentials were fit to the Buckingham form:

$$E(\text{eV}) = Ae^{-r/\rho} - C/r^6, \qquad [2]$$

where $r$ is the interatomic separation distance and $A$, $\rho$, and $C$ are semiempirical constants. $K_s$ is the core–shell spring constant in Tables 1 and 3.

The LCC potentials were fit to the orthorhombic structure (PBNM) of LCC20 (3). The LSCF potentials were simultaneously fit to three materials: LSCF6428 and LSCF2828 are cubic structures ($Pm3m$), but LSCF6482 is rhombohedral ($R\bar{3}c$). The symmetries of these space groups were maintained during all fitting. All the charges were allowed to vary during fitting for the LCC cases, so that formal charges were not maintained (Table 2). Conversely, formal charges were maintained for the La and Sr ions in the LSCF cases (Table 4). If the total charge is taken as a measure of the amount of covalency, the results indicate that these materials exhibit approximately 15–25% covalent bonding. The resulting potentials were checked by predicting the lattice constants for relevant binary oxides, such as $Cr_2O_3$ and $CrO_2$, when such data were available for comparison.

Several features are of note, as follows. First, the LCC potentials in Fig. 1 are more similar to each other than the

**TABLE 1**
**Buckingham Parameters for LCC20 Interatomic Potentials**

| Ion pair | $A$ (eV) | $\rho$ (Å) | $C$ (eV Å$^6$) | $K_s$ (eV Å$^{-2}$) |
|---|---|---|---|---|
| $La^{3+}$–O | 1527.4965 | 0.3150 | 0.00 | 78.00 |
| $Ca^{2+}$–O | 481.5355 | 0.3945 | 0.00 | 19.24 |
| $Cr^{3+}$–O | 514.8567 | 0.3838 | 0.00 | 67.00 |
| $Cr^{4+}$–O | 2562.5631 | 0.2779 | 0.00 | 72.00 |
| O–O | 22764.3000 | 0.1490 | 43.00 | 82.00 |

**TABLE 2**
**Core and Shell Charges ($|e|$) for LCC20**

| Parameter | LCC20-ox | LCC20-red |
|---|---|---|
| La core | 0.0327 | 0.0327 |
| La shell | 1.9151 | 1.8947 |
| Ca core | 0.0100 | 0.1000 |
| Ca shell | 1.9306 | 1.9068 |
| Cr3 core | 0.0050 | 0.0050 |
| Cr3 shell | 2.6690 | 2.9377 |
| Cr4 core | 0.0290 | 0.0290 |
| Cr4 shell | 4.5722 | 4.7228 |
| O core | −0.0130 | −0.0130 |
| O shell | −1.6556 | −1.6789 |

**TABLE 3**
**Buckingham Parameters for LSCF Potentials**

| Ion pair | $A$ (eV) | $\rho$ (Å) | $C$ (eV Å$^6$) | $K_s$ (eV Å$^{-2}$) |
|---|---|---|---|---|
| La–O | 1545.2100 | 0.3490 | 0.00 | 145.0 |
| Sr–O | 959.1000 | 0.3541 | 0.00 | 71.7 |
| Co–O | 327.7617 | 0.3854 | 0.00 | 196.3 |
| Fe–O | 860.5747 | 0.3083 | 0.00 | 304.7 |
| O–O | 22764.30 | 0.1490 | 43.00 | 42.0 |

LSCF potentials in Fig. 2. The similarity in Fig. 1 was identified as advantageous in prior work (2) and is easier to obtain when fitting to a single material. Fitting simultaneously to several materials of differing structures tends to disperse the potentials (Fig. 2). Second, the relative order of the potentials does not always reflect that of the ionic radii according to Shannon (24, 25). This is a correspondence sometimes sought to attain greater physical significance for such semiempirical potentials. In general, the $A$ site potentials should be higher than the $B$ site potentials. This expectation appears to be met for both LCC and LSCF in Figs. 1 and 2, although there is some overlap of $A$ site and $B$ site LCC potentials. However, the $A$ site potentials considered alone are consistently not in the proper order to reflect ionic radii. The $B$ site potentials considered alone show the proper order for the $Cr^{3+}$ and $Cr^{4+}$ in LCC, but not for the cobalt and iron in the LSCF. The reason is that data for binary oxides were available for checking the $Cr^{4+}$ potential in LCC, but not for the $Co^{4+}$ and $Fe^{4+}$ in LSCF. The latter are needed for electronic charge compensation in LSCF. Due to the lack of data for binary oxides, the cobalt and iron 4+ charge states are assumed to be adequately approximated by the Buckingham potentials for the 3+ charge states. This is clearly an important approximation and should be improved in future work. The third item of note is that the $B$ sites are slightly oxidized in the LCC20 reduced case in Table 2, which is contrary to physical expectations. These deficiencies could be improved if additional perovskite data were made available for more detailed fitting of the potentials. The last item of note is that the oxygen–oxygen Buckingham potential parameters were not varied during fitting. This potential (26) appears in many prior works using energy minimization and was left intact to enable comparisons to those results.

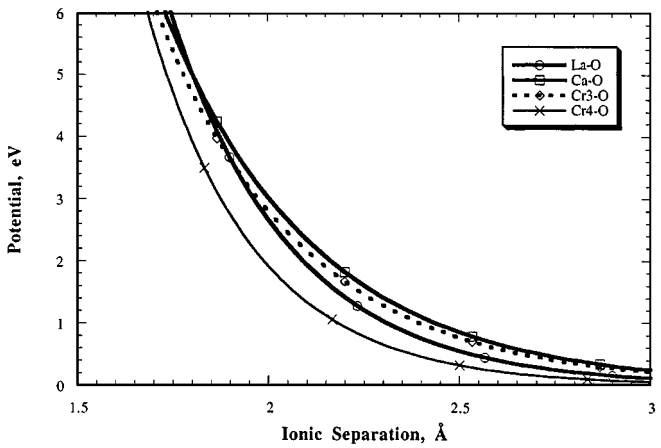


**FIG. 1.** Interatomic potentials for LCC20.

The above observations concerning the relative ordering of the potentials and the charges are indicative of the empirical nature of these techniques. The charges have essentially compensated for errors in the short-range potentials and *vice versa*. An example is the $Cr^{4+}$ effective charges in Table 2. However, the present potentials were the best available using the existing database for the perovskite crystal structures and elastic properties, despite the many fitting runs executed in several attempts to improve the physical meaning of the potentials. Note that it was not possible to reproduce the bulk modulus and thermal expansion of these materials using the formal charge potentials previously developed from simple oxides (e.g., $La_2O_3$, CaO,

**TABLE 4**
**Core–Shell Charges for LSCF Potentials**

| Ion | LSCF6428 | LSCF6482 | LSCF2828 |
|---|---|---|---|
| La core | −0.1272 | 3.1354 | 0.0012 |
| La shell | 3.1272 | −0.1354 | 2.9988 |
| Sr core | −0.1159 | 1.8910 | −0.1609 |
| Sr shell | 2.1159 | 0.1090 | 2.1609 |
| Co core | 0.4233 | −1.6578 | 0.5835 |
| Co shell | 0.8661 | 4.5378 | 0.6680 |
| Fe core | −0.6736 | 3.7340 | −1.0038 |
| Fe shell | 3.0798 | −3.6038 | 3.4550 |
| O core | 0.2297 | 0.8746 | 0.2658 |
| O shell | −1.8240 | −2.5345 | −1.7561 |

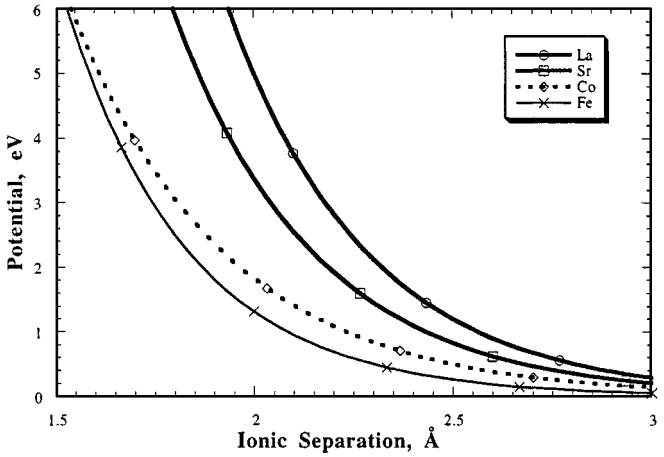


**FIG. 2.** Interatomic potentials for LSCF6428, LSCF6482, and LSCF2828.

$CrO_2$, $Cr_2O_3$) as in Refs. (2) and (3), even when partial charges were allowed in those potentials. It thus appears that a limitation of the partial charge technique may have been reached and that more extensive databases are needed for improving the potentials. A possible alternative is that recent work on strontium titanate has supplemented partial charge potentials with a Morse potential term, apparently to represent the covalent bonding contribution between the *B* sites and oxygen (1). This may be a useful technique in future work on the lanthanum-based perovskites discussed herein.

## 5. SIMULATION RESULTS AND DISCUSSION

The results of EM and MD simulations are shown in Table 5. Predictions of the unit cell volumes are reported in terms of the percentage error from the experimental values at room temperature and show good agreement except for LSCF2828. The latter may be caused by the lack of correspondence between the La and Sr potentials and the ionic radii. Predictions of the bulk moduli are within about 8% error from the experimental data. This is a noticeable improvement over formal charge models, which overpredict the bulk moduli by factors of up to 2 and thus underpredict the CTE by corresponding amounts.

**TABLE 5**
**Property Predictions with Partial Charge Potentials**

| | Property | | | |
|---|---|---|---|---|
| Material | Volume (% error) | Bulk mod. (GPa) | CTE (ppm/K) EM | CTE (ppm/K) MD |
| LCC20-ox | 0.58 | 145(136) | 7.40(10.05) | 11.77(10.05) |
| LCC20-red | 0.54 | 131(136) | 9.04(—) | 10.68(—) |
| LSCF6428 | −0.43 | 155(152) | 12.84(15.00) | 10.24(15.00) |
| LSCF6482 | −0.24 | 147(135) | — | — |
| LSCF2828 | 5.14 | 127(127) | — | — |

*Note.* Experimental data are in parentheses.

As mentioned above, two techniques were used to compute the CTE for the temperature range 0–1273 K: static free energy minimization and molecular dynamics. These simulations were performed for the LCC cases and for LSCF6428. The LSCF6482 and LSCF2828 cases exhibited structural instabilities due to the ingrowth of imaginary phonon modes during free energy minimization using the mean field EM method and were thus abandoned.

Table 5 indicates that the EM method tends to underpredict the experimental data. This may be a characteristic of the ZSISA approximation (18) used for the free energy minimization calculations and will be addressed in future work. However, the EM results for LCC appear self-consistent in that small reductions of the bulk modulus cause small increases of the CTE and *vice versa*.

The MD simulations exhibit consistency between materials. However, the CTE is slightly overpredicted for LCC and noticeably underpredicted for LSCF. These differences are due in part to the different characters of the potentials for the two materials; i.e., underpredictions of the CTE are symptomatic of formal charges, indicating that the La–O and Sr–O interactions in LSCF are also not well understood (1). The smaller potential cutoff radii for the LSCF (due to the smaller cell size) also contributes to this effect, since the sum of near field repulsions is less than for the LCC and thus the coulombic attractions could effectively stiffen the material and reduce the CTE.

Although formal charge models permit the study of defects, they are known to be deficient for predictions of thermal expansion when bonding is partially covalent. The partial charge models employed herein were an attempt to improve predictions of the bulk moduli and the CTE. Additionally, some cursory calculations of oxygen vacancy formation energies were performed to delineate the problems to be expected for defect calculations. Calculations for LSCF6428 using the Mott–Littleton technique in GULP showed that the experimental oxygen vacancy formation energy (1.28 eV in (4)) could only be reproduced with a unit cell that violated charge neutrality. The end result was that, although partial charge models can improve predictions of bulk modulus and thermal expansion, the user should be aware that defect formation energies probably cannot be treated according to the rule of charge neutrality in a defect reaction equation.

## 6. CONCLUSIONS

The results of this investigation indicate that partial charge models are advantageous for predictions of the bulk

modulus ($B$) and the CTE for perovskites. Partial charges are approximations for the partial covalency of these materials in EM and MD simulations. The EM simulations incorporated polarization via shell models and predicted $B$ to within about 8% of the experimental data, but generally underpredicted the CTE by up to 26% due to approximations in the interatomic potentials employed. MD simulations using the same potentials predicted the CTE to within 17% of experimental data for $(La,Ca)CrO_3$. MD predictions of the CTE for $(La,Sr)(Co,Fe)O_3$ were significantly lower than the experimental data due to the approximate nature of the $Co^{4+}$ and $Fe^{4+}$ interatomic potentials. Improvements in these results can be expected if more extensive databases become available for refining the potentials and effective charges. However, partial charge models do not appear applicable for the calculation of defect formation energies because crystal charge neutrality cannot, in general, be maintained.

## ACKNOWLEDGMENTS

This work was sponsored by the U.S. Department of Energy's Advanced Research and Technology Development Program. Pacific Northwest National Laboratory is operated for the U.S. Department of Energy by Battelle Memorial Institute under Contract DE-AC06-76RLO 1830. DL_POLY is a package of molecular simulation routines written by W. Smith and T. R. Forester and copyrighted by the Council for the Central Laboratory of the Research Councils, Daresbury Laboratory at Daresbury, Nr. Warrington (1996). The authors thank J. D. Gale of the Imperial College, U.K., for calculating the free energy minimizations.

## REFERENCES

1. T. Katsumata, Y. Inaguma, M. Itoh, and K. Kawamura, *Solid State Ionics* **108,** 175 (1998).
2. R. E. Williford, T. R. Armstrong, and J D. Gale, *J. Solid State Chem.* **149,** 320 (2000).
3. R. E. Williford and T. R. Armstrong, *In* "Solid Oxide Fuel Cells VI" (S. C. Singhal and M. Dokiya, Eds.), Honolulu, October 1999, The Electrochemical Society Proceedings Series, Pennington, NJ, 1999.
4. J. W. Stevenson, T. R. Armstrong, R. D. Carneim, L. R. Pederson, and W. J. Weber, *J. Electrochem. Soc.* **143**(9), 2722 (1996).
5. T. R. Armstrong, J. W. Stevenson, L. R. Pederson, and P. E. Raney, *J. Electrochem. Soc.* **143**(9), 2919 (1996).
6. T. R. Armstrong, J. W. Stevenson, K. Hasinska, and D. E. McCready, *J. Electrochem. Soc.* **145**(12), 4282 (1998).
7. W. Paulik, S. Baskaran, and T. R. Armstrong, *J. Mater. Sci.* **33,** 2398 (1998).
8. R. Nadalin and W. Brozda, *Anal. Chim. Acta* **28,** 282 (1963).
9. L. Tai, M. Nasrallah, and H. U. Anderson, *in* "Solid Oxide Fuel Cells III" (S. C. Singhal and H. Iwahara, Eds.), PV 93-4, p. 241. The Electrochemical Society Proceedings. Series, Pennington, NJ, 1993.
10. M. Cherry, M. S. Islam, J. D. Gale, and C. R. A. Catlow, *J. Phys. Chem.* **99,** 14,614 (1995).
11. M. S. Islam, M. Cherry, and C. R. A. Catlow, *J. Solid State Chem.* **124,** 230 (1996).
12. M. S. Islam, M. Cherry, and L. J. Winch, *J. Chem. Soc. Faraday Trans.* **92**(3), 479 (1996).
13. M. S. Khan, M. S. Islam, and D. R. Bates, *J. Phys Chem. B* **102,** 3099 (1998).
14. J. D. Gale, *J. Chem. Soc. Faraday Trans.* **93,** 629 (1997).
15. J. D. Gale, *Philos. Mag. B* **73,** 3 (1996).
16. B. G. Dick and A. W. Overhauser, *Phys. Rev.* **112,** 90 (1958).
17. J. D. Gale, *J. Phys. Chem. B* **102,** 5423 (1998).
18. N. L. Allen, T. H. K. Barron, and J. A. O. Bruno, *J. Chem. Phys.* **105,** 8300 (1996).
19. H. J. Monkhorst and J. D. Pack, *Phys. Rev. B* **13,** 5188 (1976).
20. N. F. Mott and M. J. Littleton, *Trans. Faraday Soc.* **34,** 485 (1938).
21. S. C. Parker and G. D. Price, *Adv. Solid State Chem.* **1,** 295 (1989).
22. T. R. Forester and W. Smith, The DL_POLY code. Daresbury Laboratory, UK, 1993.
23. M. S. D. Read, M. S. Islam, F. King, and F. E. Hancock, *J. Phys. Chem. B* **103,** 1558 (1999).
24. R. D. Shannon, *J. Appl. Phys.* **73**(1), 348 (1993).
25. R. D. Shannon and C. T. Prewitt, *Acta Crystallogr. B* **25,** 925 (1969).
26. C. R. A. Catlow, *Proc. R. Soc. A* **333,** 533 (1977).